In vivo evaluation of [18F]fluoroetanidazole as a new marker for imaging tumour hypoxia with positron emission tomography

H Barthel[1,4], H Wilson[2], DR Collingridge[1], G Brown[2], S Osman[2], SK Luthra[2], F Brady[2], P Workman[3], PM Price[1] and EO Aboagye[*,1]

[1]Cancer Research UK PET Oncology Group, Department of Cancer Medicine, Faculty of Medicine, Imperial College London, Hammersmith Hospital Campus, Du Cane Road, W12 0NN London, UK; [2]Hammersmith Imanet, Cyclotron Building, Hammersmith Hospital, Du Cane Road, W12 0NN London, UK; [3]Cancer Research UK Centre for Cancer Therapeutics, The Institute for Cancer Research, Brookes Lawley Building, Room 0E8, 15 Cotswold Road, Sutton, Surrey SM2 5NG, UK; [4]Department of Nuclear Medicine, University of Leipzig, Liebigstraße 20A, 04103 Leipzig, Germany

Development of hypoxia-targeted therapies has stimulated the search for clinically applicable noninvasive markers of tumour hypoxia. Here, we describe the validation of [18F]fluoroetanidazole ([18F]FETA) as a tumour hypoxia marker by positron emission tomography (PET). Cellular transport and retention of [18F]FETA were determined in vitro under air vs nitrogen. Biodistribution and metabolism of the radiotracer were determined in mice bearing MCF-7, RIF-1, EMT6, HT1080/26.6, and HT1080/1-3C xenografts. Dynamic PET imaging was performed on a dedicated small animal scanner. [18F]FETA, with an octanol–water partition coefficient of 0.16 ± 0.01, was selectively retained by RIF-1 cells under hypoxia compared to air (3.4- to 4.3-fold at 60 – 120 min). The radiotracer was stable in the plasma and distributed well to all the tissues studied. The 60-min tumour/muscle ratios positively correlated with the percentage of pO_2 values < 5 mmHg ($r = 0.805$, $P = 0.027$) and carbogen breathing decreased [18F]FETA-derived radioactivity levels ($P = 0.028$). In contrast, nitroreductase activity did not influence accumulation. Tumours were sufficiently visualised by PET imaging within 30 – 60 min. Higher fractional retention of [18F]FETA in HT1080/1-3C vs HT1080/26.6 tumours determined by dynamic PET imaging ($P = 0.05$) reflected higher percentage of pO_2 values < 1 mmHg ($P = 0.023$), lower vessel density ($P = 0.026$), and higher radiobiological hypoxic fraction ($P = 0.008$) of the HT1080/1-3C tumours. In conclusion, [18F]FETA shows hypoxia-dependent tumour retention and is, thus, a promising PET marker that warrants clinical evaluation.

British Journal of Cancer (2004) **90,** 2232 – 2242. doi:10.1038/sj.bjc.6601862 www.bjcancer.com
Published online 11 May 2004
© 2004 Cancer Research UK

Hypoxia occurs to a variable extent in most rodent and human solid tumours (Moulder and Rockwell, 1984; Höckel and Vaupel, 2001). It results from an inadequate and disorganised tumour vasculature and blood flow, and hence impaired oxygen delivery (Vaupel et al, 1989). Detection of hypoxia is important because hypoxia is a powerful trigger for gene expression and thus clonal selection of a more aggressive phenotype, for example, diminished apoptotic potential (Gräber et al, 1996; Koong et al, 2000). Of immediate clinical importance, hypoxia reduces local tumour control by external beam radiotherapy (Horsman and Overgaard, 1992) and predicts general treatment outcome, including metastatic potential and survival following radio/chemotherapy and surgery in a number of human cancers (Höckel et al, 1993; Brizel et al, 1996). Thus, detection of hypoxia could improve patient selection for therapy with bioreductive agents (Stratford and Workman, 1998), modified radiotherapy regimes such as acceler-ated radiotherapy with carbogen and nicotinamide 'ARCON' (Hoskin and Saunders, 1994), conformal radiotherapy, and hypoxia-targeted gene therapy (Dachs et al, 1997). Beyond oncology, potential applications exist for diagnosis of stroke, ischemic heart disease, peripheral vascular disease, arthritis, and anaerobic infection.

Studies with fine needle oxygen electrodes provided proof that low pO_2 leads to poor outcome after treatment (Höckel et al, 1996; Brizel et al, 1997; Nordsmark and Overgaard, 2000; Fyles et al, 2002). Immunohistochemical parameters obtained by staining biopsy sections with antibodies to EF5, pimonidazole, hypoxia-inducible factor 1α (HIF-$1\alpha^3$), and carbonic anhydrase IX have also shown promise (Evans et al, 1996; Wykoff et al, 2000; Aebersold et al, 2001; Kaanders et al, 2002). Utility in a routine clinical setting would, however, favour a simple, convenient, noninvasive method for detecting tumour hypoxia that yields results, which correlate with clinical outcome. In this regard, a number of probes have been developed for imaging hypoxia by positron emission tomography (PET) and single-photon emission tomography in nuclear medicine. These include 18F-labelled 2-nitroimidazoles such as [18F]FMISO (Koh et al, 1995; Rasey et al, 1996), [18F]EF5 (Ziemer et al, 2003), [18F]FETNIM (Yang et al, 1995), [18F]FAZA (Sorger et al, 2003), and N-(2-([18F]fluoroethyl)-2-(2-nitro-imidazol-1-yl)-acetamide ([18F]FETA) (Rasey et al, 1999); copper

*Correspondence: Dr EO Aboagye, Molecular Therapy Group, Faculty of Medicine, Imperial College London, Hammersmith Hospital Campus, Du Cane Road, London W12 0NN, UK;
E-mail: eric.aboagye@imperial.ac.uk

bis-thiosemi-carbazones such as [^{60}Cu]ATSM (Fujibayashi *et al*, 1997; Dehdashti *et al*, 2003); technetium-based probes such as [^{99m}Tc]HL-91 (Honess *et al*, 1998); and iodine-based probes such as [^{123}I]IAZA (Mannan *et al*, 1991). Due to various limitations, none of these radiotracers have found their way into routine clinical use (Workman and Brown, 1981; Nunn *et al*, 1995; Rasey *et al*, 1999; Bentzen *et al*, 2002).

Of the numerous possibilities in nuclear medicine, appropriately labelled 2-nitroimidazole probes are particularly attractive for imaging tumour hypoxia (pO_2 <10 mmHg (Höckel *et al*, 1996; Nordsmark *et al*, 1996); radiobiological hypoxia, pO_2 <1 mmHg (Rasey *et al*, 1990)). A combination of pharmacological and physical properties that need to be considered as part of an ideal design goal include: (i) a nitro group with appropriate redox potential ($E_{1/7}$ of ~ −380 to −390 mV) for selective reduction and binding in hypoxic tumour cells; (ii) lipophilicity that is high enough to enable diffusion across cellular membranes to the site of metabolism (octanol–water partition coefficient of ~ ≥0.1 (Brown and Workman, 1980; Workman, 1982), but low enough (~ ≤2) to assure rapid systemic elimination and, hence, convenient imaging times (within 2 h); (iii) stability to hypoxia-independent degradation; and (iv) high photon flux (and low energy) to assure high detection sensitivity and spatial image resolution. The last property would favour ^{18}F-based PET radio-tracers. In this manuscript we report on preclinical studies that underpin the development of [^{18}F]FETA ([^{18}F]fluoroetanidazole), an extremely promising hypoxia probe for imaging by PET. We demonstrate for the first time in mouse models of cancer that the retention of [^{18}F]FETA-derived radioactivity correlates with pO_2 and radiation sensitivity.

MATERIALS AND METHODS

Radiosynthesis of [^{18}F]FETA

Unless otherwise noted, all reagents, including anhydrous solvents, were obtained from Sigma-Aldrich (Poole, UK). The synthesis of [^{18}F]FETA was based on the method of Tewson (1997), with some modifications. N-[2-(toluene-4-sulphonyloxy)-ethyl]-phtha-limide (I in Figure 1) was prepared according to the literature method (Tewson, 1997). The precursor, 2,3,5,6-Tetrafluorophenyl 2-(2-nitroimidazol-1-yl) acetate, (II) was prepared by a novel method, published separately (Wilson, 2003). [^{18}F]fluoride was prepared by the ^{18}O$(p,n)^{18}$F reaction using H$_2^{18}$O enriched water (Ruth and Wolf, 1979). A measure of 250 μl 0.1 M K$_2$CO$_3$ and 3 mg [2,2,2]Kryptofix in 500 μl acetonitrile were added to the [^{18}F]fluoride. The fluoride was dried in a glassy carbon vessel at 125°C, under N$_2$, for 35 min (with two further additions of 500 μl acetonitrile), before cooling. In total, 15 mg of compound (I) was dissolved in 500 μl acetonitrile. This was added to the reaction vessel, which was sealed at 100°C for 10 min before evaporation of the acetonitrile. A measure of 75 μl hydrazine hydrate was added to the reaction vessel. [^{18}F]fluoroethylamine (IV) was distilled from the reaction vessel (75°C, N$_2$ flow ~3 ml min^{-1}) into a vial containing 4 mg precursor (II) in 400 μl of ice cold acetonitrile. The vial was sealed and stirred for 30 min at room temperature. The resulting product was purified by high-performance liquid chromatography (HPLC) (Waters μ-Bondapak C$_{18}$ column) and eluted with water (Baxter Healthcare Ltd, Compton, UK; 3 ml min^{-1}). The radioactive product having the same retention time as fluoroetanidazole was collected (reference material synthesised according to Tewson, 1997). The product was evaporated to dryness and taken up in 0.9% saline (Phoenix Pharma Ltd, Gloucester, UK) for injection. The (manual) preparation time for [^{18}F]FETA (synthesis, purification, formulation) from the end of bombardment was approximately 3 h.
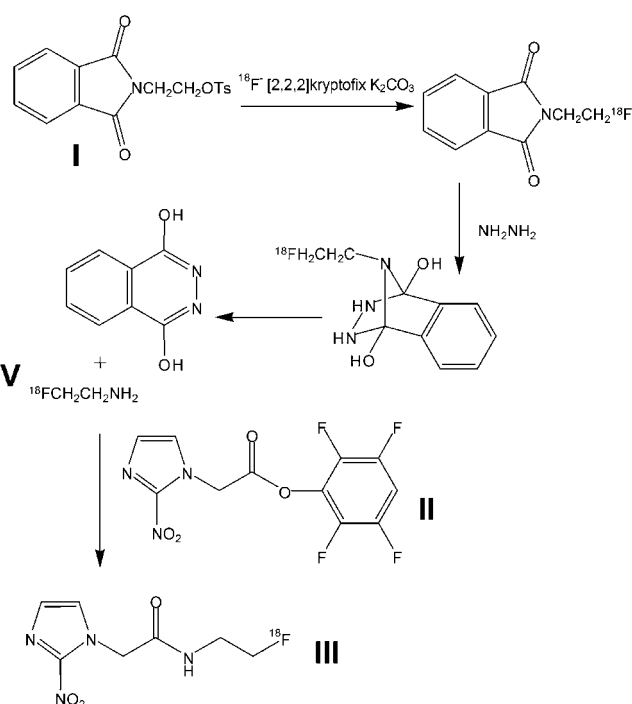

Figure 1 Radiochemical synthesis of [^{18}F]FETA. I, II, III, and IV represent N-[2-(toluene-4-sulphonyloxy)-ethyl]-phthalimide, 2,3,5,6-Tetrafluorophenyl 2-(2-nitroimidazol-1-yl) acetate, [^{18}F]Fluoroetanidazole, and [^{18}F]Fluoro-ethylamine.

Lipophilicity measurements

The lipophilicity of [^{18}F]FETA was determined by measuring the octanol–water partition coefficient. For this, 80–100 μCi (2.96–3.70 MBq) of [^{18}F]FETA was dissolved in distilled H$_2$O to a final volume of 0.5 ml and 0.5 ml of octan-1-ol (BDH Chemicals Ltd, Poole, UK) was added. The resulting mixture was processed in an orbital shaker (Sanyo Gallenkamp PLC, Loughborough, UK) for 10 min at 300 rpm and subsequently centrifuged for 30 min (12 000 rpm; Rotina 35R, Hettich Zentrifugen, Tuttlingen, Germany). Aliquots (200 μl) of the resulting top layer (representing [^{18}F]FETA dissolved in octanol) and bottom layer ([^{18}F]FETA dissolved in H$_2$O) were taken and the radioactivity in these samples was measured using a Cobra II Auto-Gamma counter (Packard Instruments, Meriden, CT, USA). Six octanol–H$_2$O mixtures were analysed and the complete experiment was repeated once. The octanol–water partition coefficient was calculated by dividing the octanol-containing radioactivity by the water-containing radioactivity.

Cellular uptake of [^{18}F]FETA

The inhibitory effect of oxygen on [^{18}F]FETA uptake by cells was studied *in vitro* in RIF-1 tumour cells. Uptake was defined as the transport of radiotracer into cells and its specific binding to cellular macromolecules (and glutathione). The cells were cultured (5% CO$_2$ incubator at 37°C) in T75 flasks in RPMI growth medium (Life Technologies, Strathclyde, UK) supplemented with 10% foetal bovine serum (Sigma) and antibiotics. Exponentially growing cells were harvested, dissolved in phosphate-buffered saline (PBS) and placed in a custom-made hypoxic chamber (Aboagye *et al*, 1997a), which was positioned in a 37°C shaking water bath and incubated with pure nitrogen (O$_2$ <20 ppm; BOC Gases, Guildford, UK) or with air as control, each flowing at 2 l min^{-1}. After pregassing for 8 min, the cells were incubated with 80–100 μCi (2.96–3.7 MBq) of

[^{18}F]FETA. No correction for the total amount of stable etanidazole in the reaction mixture was made between experiments. Immediately after addition of the radioactivity, and at 15, 30, 45, 60, 90, and 120 min, the cells were harvested and centrifuged (5000 rpm for 5 min) to obtain a pellet. The pellet was washed twice with PBS (5 ml) and centrifuged as above. The cell number in the resulting pellet was determined by counting cells that excluded trypan blue. The total radioactivity added to each hypoxic chamber and the cell-bound radioactivity were measured on a Cobra II Auto-Gamma counter (Packard Instruments, Meriden, Connecticut, SA, USA) to determine the degree of radioactivity binding. Percentage of bound radioactivity was calculated as (bound radioactivity in 10^6 cells $\times$ 100)/total radioactivity. These experiments were carried out in triplicate and repeated independently three times.

Animals and tumours

The mice used in this work were obtained from Harlan UK Ltd (Bicester, UK). To obtain tumours, $2 \times 10^5 - 2 \times 10^6$ tumour cells harvested from exponentially growing *in vitro* cultures were injected into the dorsum subcutis of normal C3H/Hej and Balb/c mice (for RIF-1 mouse fibrosarcoma and EMT6 mouse mammary carcinoma tumours, respectively) or Balb/c nude mice (for HT1080 human fibrosarcoma and MCF-7 human mammary carcinoma tumours). In the case of the HT1080 tumours, two subclones (1-3C, 26.6) with different capacities for producing vascular endothelial growth factor (VEFG) were studied. As published recently by our group, the 26.6-subclone produces two- to four-fold more VEGF than the 1-3C-subclone (Collingridge et al, 2002). To obtain MCF7 tumours, a 60-day slow release 17-β-oestradiol pellet (Innovative Research of America, Sarasota, FL, USA; 0.72 mg pellet^{-1}) was inserted subcutaneously on the contralateral flank of the mouse at the time of inoculation of the tumour cells to maintain blood levels of 300 – 400 pg ml^{-1}. All the animal work was performed by licensed investigators in accordance with the United Kingdom's 'Guidance on the Operation of Animals (Scientific Procedures) Act 1986' (HMSO, London, UK, 1990) and in full compliance with government regulations and the UKCCCR guidelines on animal welfare in experimental neoplasia (Workman et al, 1998). Tumours were selected for experiments when they had reached 5 – 8 mm in diameter (100 – 300 mg). In order to obtain comparable results, all biodistribution studies, PET imaging studies, and pO_2 measurements were performed in anaesthetised mice. For that, a general neuropleptanalgesia comprising of a mixture of fentanyl citrate/fluanisone (Janssen-Cilag Ltd, Saunderton, UK; 0.79 and 25 mg kg^{-1} respectively) and midazolam hydrochloride (Phoenix Pharma, Ltd, Gloucester, UK; 12.5 mg kg^{-1}) was injected i.p. 5 min before the start of the experiments. Irradiation of mice, in studies to determine radiobiological hypoxic fraction, were performed in unanaesthetised mice.

Biodistribution of [^{18}F]FETA

Anaesthetised tumour-bearing mice were injected intravenously via the lateral tail vein with 100 μl of [^{18}F]FETA (10 – 100 μCi; 0.37 – 3.7 MBq). Mice were killed by exsanguination via cardiac puncture 60 min after injection of the radiotracer. Aliquots of heparinised blood were rapidly centrifuged (2000 **g** for 5 min) to obtain plasma. The radioactivity contained in tumour, liver, kidney, spleen, lungs, heart, small intestines, brain, muscle, bone, blood, plasma, faeces, and urine was determined in a Cobra II Auto-Gamma counter and expressed as % ID g^{-1} (percentage of injected dose per gram of tissue). A minimum of six mice was used for each tumour model.

Biodistribution studies were also carried out in mice following modulation of tumour hypoxia. In RIF-1 tumour-bearing mice, the degree of tumour hypoxia was modulated by administration of carbogen gas (95% O$_2$, 5% CO$_2$), which is known to decrease tumour hypoxia (Powell et al, 1999). There are a number of reports

in the literature demonstrating an increase in oxygenation or perfusion in RIF-1 tumours under carbogen breathing. These studies include direct pO_2 measurements, as well as magnetic resonance and ^{86}Rb extraction methods in RIF-1 tumours implanted in the leg (Hasegawa et al, 1987; Song et al, 1987; Ilangovan et al, 2002) or flank (Helmer et al, 1998; Dardzinski and Sotak 1994; Honess and Bleehen, 1995). Carbogen gas was delivered via a nose cone at 2.0 l min^{-1}, starting 2 min before radiotracer injection and for 60 min after radiotracer injection ($n = 5$). Untreated RIF-1 tumour-bearing mice served as controls ($n = 8$). Mice were injected with [^{18}F]FETA and killed at 60 min postinjection (p.i.), as described above. Successful modulation of tumour pO_2 was verified by means of OxyLite probes as described below.

Small animal [^{18}F]FETA-PET imaging

In parallel with the 60-min biodistribution studies above, the time course of [^{18}F]FETA distribution was studied *in vivo* in tumour-bearing mice by means of a second-generation dedicated small animal PET scanner (Quad-HIDAC; Oxford Positron Systems, Weston-on-the-Green, UK (Jeavons et al, 1999)). Mice were anaesthetised as described above and placed prone on a thermostatically controlled bed within the scanner. All anaesthetised animals (in the PET imaging, biodistribution and OxyLite pO_2 studies) were placed on thermal platforms to maintain their body temperature at $\sim$37°C. Dynamic PET scans were acquired over 60 min after intravenous (i.v.) injection of 40 – 100 μCi (1.48 – 3.7 MBq) of [^{18}F]FETA via a tail vein cannula. The imaging and image-data processing protocol has been recently described in detail elsewhere (Barthel et al, 2003). In brief, data were acquired in list mode format and image reconstruction was performed by filtered back-projection using a 2D Hamming filter (cutoff 0.6). The image data sets obtained were transferred to a SUN workstation (Ultra 10; SUN Microsystems, Santa Clara, CA, USA) and visualised using the ANALYZE software (Version 5.0; Biomedical Imaging Resource, Mayo Clinic, Rochester, NY, USA). Region(s) of interest (ROIs) were defined for tumour and heart cavity (to provide information on the delivered radioactivity) on three to six transverse planes for tumour and three planes for heart cavity. Time vs radioactivity curve(s) (TACs) from the ROIs were averaged for each tumour and normalised to the integral of the heart cavity TAC. Altogether, four HT1080/1-3C and three HT1080/26.6 tumour-bearing mice were scanned.

In vivo metabolism of [^{18}F]FETA

Plasma, urine, liver, gall bladder, muscle, and tumour samples obtained from RIF-1 tumour-bearing C3H/Hej mice were assessed for putative [^{18}F]FETA metabolites by HPLC. For this, plasma samples (100 μl) were deproteinated by adding 2.0 ml ice-cold methanol and centrifuged (3000 **g**, 10 min, 4°C). Liver, muscle, and tumour samples were cut into small pieces and homogenised in 2.0 ml of ice-cold methanol using an Ultra-Thurrax homogeniser (IKA, Staufen, Germany) and the resultant homogenate was centrifuged (3000 g, 10 min, 4°C). The supernatants from plasma and tissues were evaporated to dryness in a rotary evaporator (50°C) under vacuum, reconstituted in 1.5 ml of mobile phase (methanol/H$_2$O (20/80% v v^{-1})), centrifuged and filtered (0.2 μm). Unlike plasma and tissue samples, urine and gall bladder samples were diluted with 1.5 ml of mobile phase and clarified by filtration (0.2 μm). Aliquots of each filtrate (1.0 ml) and of the injected dose solution diluted in 1.5 ml of mobile phase were analysed by HPLC. The samples were separated on a C$_{18}$ μBondapak column (7.8 $\times$ 300 mm, size 10 μm; Waters, Milford, MA, USA) that was eluted with the aforementioned mobile phase at a flow rate of 2.0 ml min^{-1}. The radioactivity of the eluents was monitored. Peak

areas were integrated and corrected for physical decay and background radioactivity.

Direct measurement of pO_2

Oxygenation in the established tumour models was measured using the OxyLite pO_2 system (Oxford Optronix Ltd, Oxford, UK) (Young et al, 1996; Collingridge et al, 1997; Seddon et al, 2001). The OxyLite probes measure pO_2 by using a fluorescence quenching technique (Young et al, 1996). These experiments were performed under general neuroleptanalgesia. The animals were placed on a thermal blanket (37°C) and a maximum of four (depending on the tumour size) oxygen probes were simultaneously implanted into the mouse tumours. The probes were moved forward manually ∼0.2 cm every 10 min (total measurement time 30–50 min), which resulted in 45–125 pO_2 measurements per tumour. All oxygen measurements were postcalibrated to account for tumour temperature, as previously reported (Young et al, 1996; Collingridge et al, 1997).

Measurement of vessel density

In parallel studies in HT1080 (grown from 1-3C and 26.6 subclones) tumour-bearing mice, tumours were excised for histological examination of vessel density. For this, each of seven 1-3C and 26.6 tumours were excised, fixed in formalin, embedded in paraffin, and cut into 5.0 μm sections. Adjacent sections were stained with haematoxylin–eosin (H&E). Sections from three different regions of each tumour, separated by at least 1.0 mm, were used for the analyses. Vessels were counted in five randomly selected fields of view (0.23 mm^2) per section using a BX51 Olympus microscope (Olympus Optical, Tokyo, Japan) at ×200 magnification.

Determination of radiobiological hypoxic fraction

In addition to the pO_2 measurements, radiobiological hypoxia was evaluated for the 26.6. and 1-3C subclones of the HT1080 tumours by performing clonogenic assays. Clonogenic cell survival, which is still regarded as gold standard for measuring tumour hypoxia (Rockwell and Moulder, 1990), was determined using an established protocol (Collingridge and Rockwell, 2000). In brief, the tumour-bearing mice were irradiated with 5, 15, or 25 Gy (mean dose rate = 4.3 Gy min^{-1}) using an IBL 637 irradiator (CIS bio international, Gif/Yvette Cedex, France). One group of mice breathed air during the irradiation; the other group comprised of mice killed 10 min before the irradiation ($n = 12$ per group). Immediately following irradiation, the tumours were excised, minced, and digested for 45 min in a 37°C shaking water bath with a 10 ml solution of foetal bovine serum-free RPMI growth medium containing 2 mg ml^{-1} collagenase type IV (Sigma, Poole, UK) and 0.2 mg ml^{-1} DNAse I (Sigma). After centrifugation, cell density was determined by trypan blue exclusion and defined numbers of cells were plated in Petri dishes containing complete growth medium. The dishes were incubated at 37°C in a humidified incubator in an atmosphere of 95% air/5% CO_2 for 10–14 days. The resulting colonies were fixed and stained with crystal violet made up in 70% ethanol and subsequently counted. The survival fraction was calculated by dividing the plating efficiency of the irradiated mice by that of unirradiated control mice ($n = 4$). Using these survival curves, radiobiological hypoxia fraction was calculated from the vertical displacement of the aerobic curve from the anoxic curve according to the equation $\log_{\text{hypoxia fraction}} = \log_{\text{aerobic survival fraction}} - \log_{\text{anoxic survival fraction}}$ (Moulder and Rockwell, 1984). The determination of hypoxic fraction in this way is only possible if the survival curves are parallel. Pooled tumours from four animals were used for each irradiation level and tumour type.

Nitroreductase activity

Tumour retention of an ideal radiolabelled 2-nitroimidazole should depend solely on intratumoural oxygenation levels, and not on the levels of nitroreductase activities. In this regard, we investigated the influence of tumour nitroreductase activities on [^{18}F]FETA tumour retention. The activities of cytochrome $P450$ reductase, cytochrome b_5 reductase, and DT-diaphorase were determined in excised, snap-frozen tumours using a standard cytochrome c assay, as previously described by Sharp et al (2000). Briefly, enzyme activities were determined on a UV-spectrophotometer (BioMate 5; Thermo Spectronic, Cambridge, UK) by measuring the rate of reduction of cytochrome c at 550 nm (Walton et al, 1991). Tumour samples were thawed and homogenised in an equivalent volume of 50 mM Tris – 150 mM KCl – HCl buffer (pH 7.4). The homogenates were centrifuged (10 000 rpm for 30 min, 4°C) and the resulting supernatant, which represented the S9 fraction, was taken for the further analysis. The protein content of the S9 fractions was determined using a commercial kit (BCA protein assay kit; Pierce, Rockford, IL, USA). Samples of the S9 fraction (5–30 μl) were added to 1 ml of a reaction mixture containing 50 mM (final concentration) Tris HCl buffer (pH 7.4), 20 μM menadione (Sigma) as initial electron acceptor, 70 μM cytochrome c (Sigma) as terminal electron acceptor, 200 μM NADH (Sigma) as electron donor, and 1.4 mg ml^{-1} bovine albumin fraction V (Sigma). The solutions were prewarmed at 37°C and the experiment was performed with or without 10 μM dicumarol (Sigma), an established inhibitor of DT-diaphorase (Hollander and Ernster, 1975). DT-diaphorase activity was taken as dicumarol-inhibitable activity and expressed as nmol of cytochrome c reduced per minute per mg of protein. The activities of cytochrome $P450$ reductase and cytochrome b_5 reductase were determined as above, but without menadione/dicumarol, and with 200 μM NADPH (Sigma) instead of NADH in the case of cytochrome $P450$ reductase assay (Fitzsimmons et al, 1996; Winski et al, 1998).

Statistics

Statistical analyses were performed using the software SPSS for Windows, version 10.0.7 (SPSS Inc., Chicago, IL, USA). Differences in pO_2 data, ex vivo [^{18}F]FETA biodistribution, and nitroreductase activities were tested for significance using analysis of variance (ANOVA). Two-sided Student's t-test for independent samples was employed to test for differences in [^{18}F]FETA uptake in vitro under normoxic and hypoxic conditions, pO_2 values, and ex vivo [^{18}F]FETA retention in RIF-1 tumours treated with carbogen vs untreated controls, as well as differences between vessel density, clonogenic survival, and fractional radiotracer retention obtained from dynamic PET scanning in 26.6 and 1-3C subclones of HT1080 tumours. Associations between [^{18}F]FETA tumour retention, pO_2 values, and nitroreductase activities in the established tumour models were tested for correlations by means of linear regression analysis. pO_2 values obtained from the OxyLite measurements were expressed as median values for all investigated mouse tumours. Survival fractions from clonogenic assays were calculated relative to the corresponding plating efficiency and are given as mean $\pm$ 1 s.e.m. Survival curves were fitted by regression analysis and compared at the midpoints of the curves. Unless stated, data are expressed as mean $\pm$ 1 s.e.m. The P-values of $\leqslant 0.05$ were considered significant.

RESULTS

Radiochemistry and in vitro characteristics of [^{18}F]FETA

Beginning with 30–50 mCi (1.11–1.85 GBq) [^{18}F]fluoride, [^{18}F]FETA yields were typically 0.6–3.0 mCi (22–111 MBq), which

represents a final (decay corrected to end of bombardment) radiochemical yield of approximately 10–20%. High-performance liquid chromatography analyses of the [^{18}F]FETA dose solutions were performed 60 min after preparation of the radiotracer. [^{18}F]FETA eluted at ~9.5 min. The radiochemical purity was 94.6 $\pm$ 1.5% ($n = 4$). The lipophilicity of [^{18}F]FETA expressed as octanol–water partition coefficient was determined to be 0.16 $\pm$ 0.01 ($n = 12$).

We studied the uptake of [^{18}F]FETA in air vs nitrogen in RIF-1 cells. The uptake of the radiotracer by normoxic cells was very low. In contrast, there was a rapid time-dependent linear increase of [^{18}F]FETA uptake by RIF-1 cells under nitrogen, which was 3.0- and 4.3-fold as compared to the normoxia values at 60 and 120 min p.i., respectively. In this model system the hypoxia-dependent increase in [^{18}F]FETA uptake reached significance after 60 min (Figure 2).

In vivo tissue distribution and metabolism of [^{18}F]FETA

The normal tissue retention of the radiotracer at 60 min postinjection was low ($<5\%$ ID g^{-1}) in lung, heart, brain, and bone; intermediate (5–8% ID g^{-1}) in plasma, liver, spleen, small intestines, and muscle; and high ($>8\%$ ID g^{-1}) in kidney, bile, and urine (Figure 3). The 60-min tumour retention of [^{18}F]FETA ranged from 6 to 10% ID g^{-1} for the different xenografts ($P = 0.023$; one-factorial ANOVA; Figure 3 inset). Other than differences in tumour retention, no significant differences in radiotracer accumulation were found for normal tissues of the different mouse strains (data not shown).

Radiochromatograms of plasma, liver, tumour, muscle, gall bladder, and urine that were obtained at 10 (plasma, liver, and tumour) and 60 min (all tissues and body fluids) after the administration of [^{18}F]FETA are shown in Figure 4. As with the analysis of the dose solution, the parent compound ([^{18}F]FETA) eluted at a retention time of ~9.5 min. Parent [^{18}F]FETA comprised 88% of the total radioactivity in plasma at 10 min p.i. In tumour, a minor radioactive peak at a retention time of ~6 min that comprised 18% of the total radioactivity was detected at 10 min p.i., whereas most of the radioactivity (92%) in the liver was associated with the metabolite(s) eluting at ~6 min. At 60 min p.i., metabolite peaks with retention times
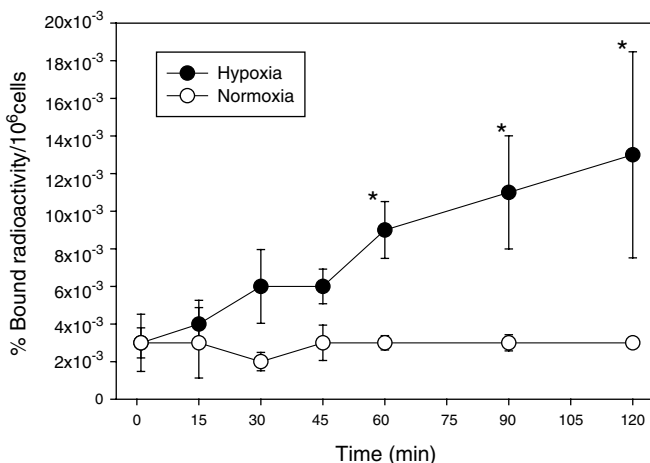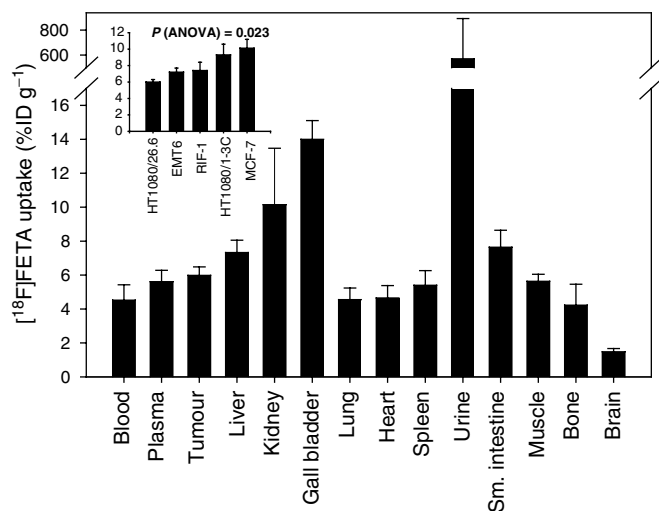

Figure 3 Tumour and normal tissue distribution of [^{18}F]FETA at 1 h p.i. in HT1080/26.6 tumour-bearing male Balb/c nu/nu mice ($n = 10$). Inset: radiotracer uptake in the different tumour types ($n = 5$–10). Data are mean % ID g^{-1} $\pm$ s.e.m.

of ~6 to 7 min were detected in the plasma (7% of total radioactivity), muscle (50%), liver (99%), bile (82%), tumour (52%), and urine (26%) (Figure 4). These HPLC data represent profiles of soluble parent and metabolites. The acid-insoluble fraction obtained from PCA extraction (representing bound radioactivity) was 69.2% for tumour and 63.7% for liver tissues at 60 min p.i.

[^{18}F]FETA tumour retention correlates with pO_2 but not nitroreductase activity

Various threshold pO_2 values (<1, 2.5, 5, and 10 mmHg) have been used to describe the degree of hypoxia in tissues. In the tumour xenografts used here, the relative frequency of pO_2 values <1.0 mmHg as determined by the OxyLite method ranged from 28 ± 13 to $93 \pm 9\%$ ($P = 0.008$; one-factorial ANOVA). The relative frequency of pO_2 values <2.5 mmHg ranged from 51 ± 13 to $100 \pm 0\%$ ($P = 0.057$). In HT1080 tumours, the relative frequency of hypoxic pO_2 values was significantly higher for the 1-3C subclone compared to the 26.6 subclone at a cutoff pO_2 of 1.0 mmHg (93 ± 9 vs $55 \pm 15\%$; $P = 0.023$) and 2.5 mmHg (100 ± 0 vs $66 \pm 16\%$; $P = 0.045$).

For all the tumour models, the relative [^{18}F]FETA retention, expressed as tumour-to-muscle ratio, was positively correlated with the relative frequency of pO_2 values <5 mmHg. This correlation was found to be linear ($y = 0.04x - 1.5$, $r = 0.805$) and significant ($P = 0.027$; Figure 5A). A trend towards a significant positive correlation was also observed for the association between tumour [^{18}F]FETA retention and relative frequency of pO_2 values <2.5 mmHg ($r = 0.691$, $P = 0.064$; Figure 5B). Of interest, [^{18}F]FETA radiotracer retention at 60 min p.i. was higher in the less VEGF-producing HT1080/1-3C subclone compared to the 26.6 subclone (9.29 ± 1.36 vs $5.98 \pm 0.50\%$ ID g^{-1}; $P = 0.015$). In addition, tumour/muscle ratios obtained from the [^{18}F]FETA biodistribution studies were significantly higher for the 1-3C subclone as compared to the 26.6 subclone (1.94 ± 0.36 vs 1.05 ± 0.03, $P < 0.001$).

The activities of cytochrome $P450$ reductase, cytochrome $b5$ reductase, and DT-diaphorase for the different tumours are given in Table 1. There were significant intertumour differences (one-factorial ANOVA) in enzyme activity. The range of these values, however, were ≤ 2.5 fold for all the reductive
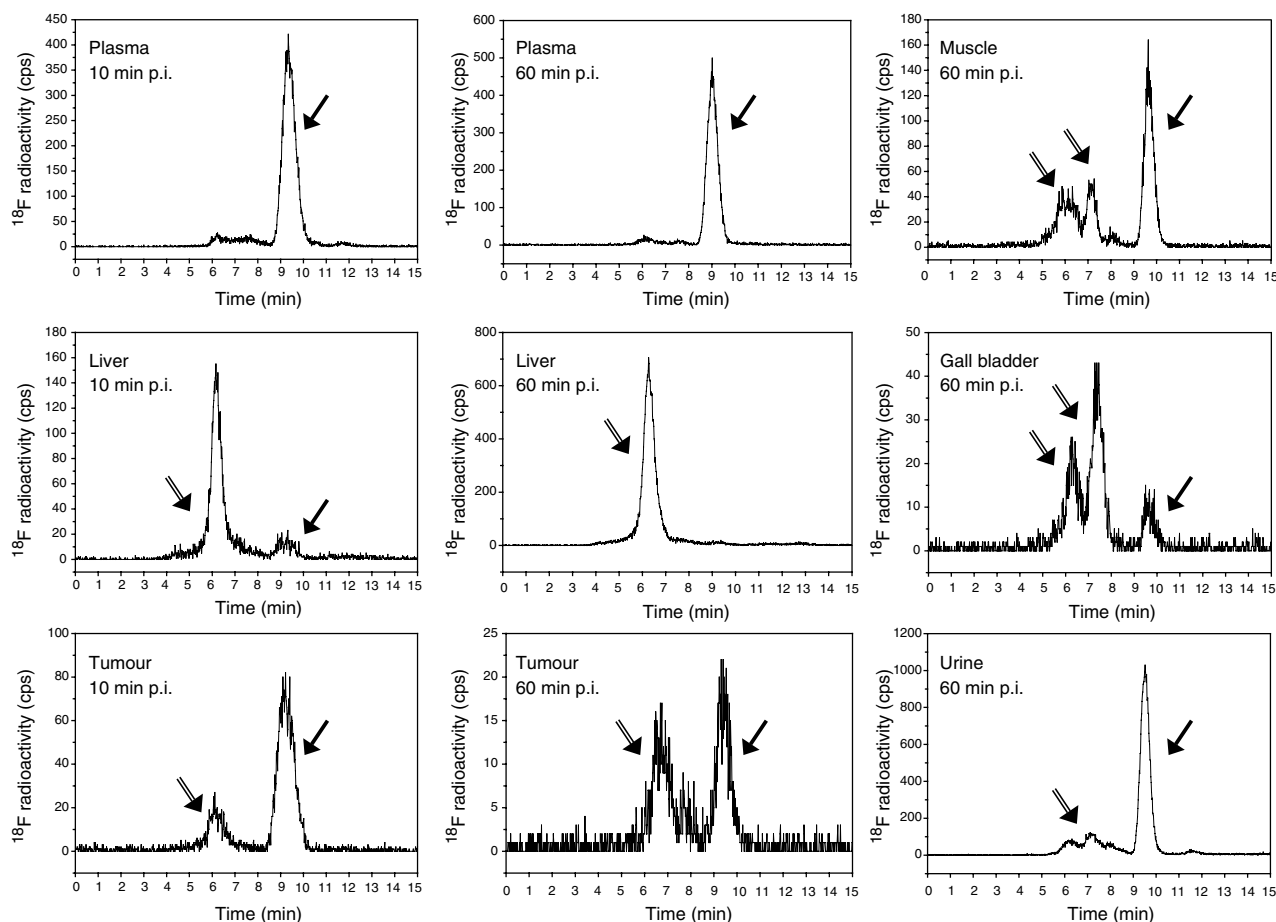

Figure 2 In vitro binding of [^{18}F]FETA to RIF-1 cells under hypoxic (-●-) and normoxic (-○-) conditions. The cells were incubated with [^{18}F]FETA under nitrogen gas or air for 0–120 min and washed to remove unbound radioactivity. The percentage of bound radioactivity was calculated as (bound radioactivity in 10^6 cells × 100)/total radioactivity. Data are mean $\pm$ s.e.m. ($n = 3$), *$P \leq 0.05$.

Figure 4 Reversed-phase high-performance liquid chromatograms of [^{18}F]FETA and its putative metabolites at an early time-point (10 min p.i.) in plasma (**A**), liver (**D**), and tumour (**G**), and a late time-point (60 min p.i.) in plasma (**B**), muscle (**C**), liver (**E**), gall bladder (**F**), tumour (**H**), and urine (**I**). Filled arrows are parent [^{18}F]FETA compound, and double-lined arrows are metabolites.
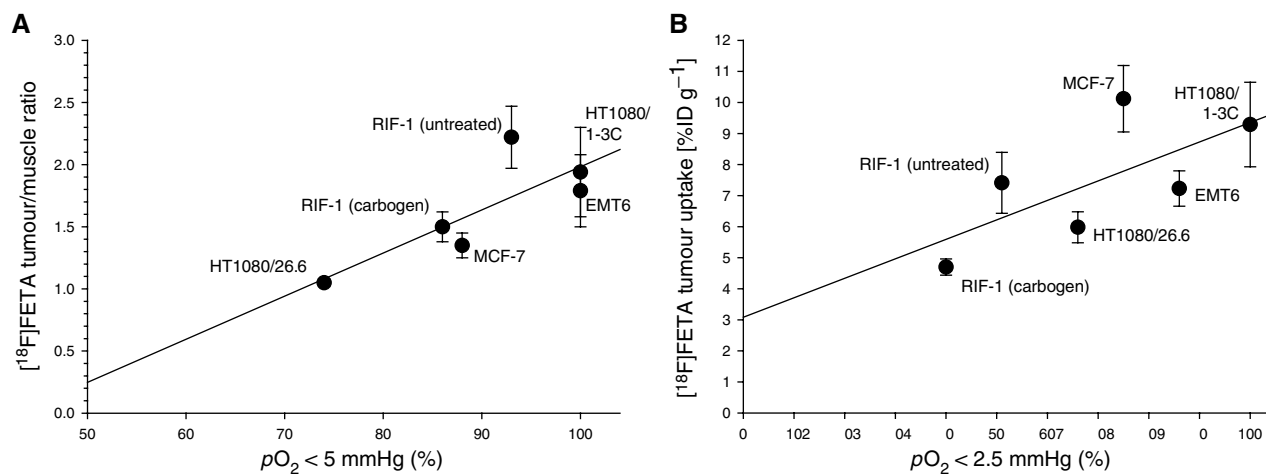

Figure 5 Association between tumour oxygenation as measured by OxyLite probes and [^{18}F]FETA tumour uptake determined by *ex vivo* biodistribution studies. (**A**) Relative [^{18}F]FETA uptake expressed as tumour-to-muscle ratio *vs* relative frequency of pO_2 values <5 mmHg. (**B**) [^{18}F]FETA uptake *vs* relative frequency of pO_2 values <2.5 mmHg.

enzymes tested (Table 1). There were no correlations between tumour enzyme profiles (cytochrome P450 reductase, cytochrome b5 reductase, and DT-diaphorase) and *ex vivo* [^{18}F]FETA tumour retention or tumour pO_2 obtained from OyxLite measurements.

Acute changes in pO_2 are detectable with [^{18}F]FETA

The ability to detect acute changes in tumour oxygenation was investigated in RIF-1 tumours after application of a physiological modulator, for which the resultant effect is well documented.

Table 1 Nitroreductase activities in established tumours

Tumour type	Cytochrome P450 reductase (nmol min^{-1} mg^{-1})	Cytochrome b5 reductase (nmol min^{-1} mg^{-1})	DT-diaphorase (nmol min^{-1} mg^{-1})
RIF-1	2.21 ± 0.18	50.0 ± 1.8	1.38 ± 0.23
HT1080/26.6	3.39 ± 0.36	36.8 ± 1.4	0.93 ± 0.01
HT1080/1-3C	4.15 ± 0.34	35.3 ± 2.5	0.21 ± 0.05
EMT6	2.79 ± 0.37	52.2 ± 1.9	0.62 ± 0.15
MCF-7	2.01 ± 0.17	20.8 ± 1.0	0.00 ± 0.00[a]
P (ANOVA)	0.001	<0.001	<0.001

Enzyme activities were determined spectroscopically by measuring reduction of cytochrome c at 550 nm, as described in Materials and Methods. Units are nmol of cytochrome c reduced per minute per mg of sample protein and are given as mean ± s.e.m. ($n = 5-7$). [a]No activity detected within effective range of assay (lower limit of detection = 0.05 nmol min^{-1} mg^{-1}).

Carbogen breathing decreased [^{18}F]FETA tumour retention to 4.70 ± 0.26% ID g^{-1}, compared to untreated controls (7.41 ± 0.98% ID g^{-1}; $P = 0.028$). In tissues other than tumours, [^{18}F]FETA retention was not altered by carbogen breathing. Administration of carbogen decreased the relative frequency of pO_2 values <2.5 mmHg in comparison to untreated controls (40 ± 11 vs 51 ± 13%). However, these differences did not reach significance level ($P = 0.551$).

Small animal PET imaging with [^{18}F]FETA

Whole body PET scanning was carried out in HT1080/26.6 ($n = 3$) and HT1080/1-3C tumour-bearing mice ($n = 4$). For illustration purposes, the 30–60 min summed images are presented (Figure 6). In agreement with the biodistribution data determined by *ex vivo* γ-counting, the PET images revealed high [^{18}F]FETA accumulation in tumour, kidney, urinary bladder, and proximal parts of the small intestine (Figure 6A). In contrast, radiotracer retention was low in brain and spinal cord (Figure 6B). Also in agreement with the biodistribution studies, the tumour retention of [^{18}F]FETA was higher in all HT1080/1-3C tumours (Figure 6C) than in the HT1080/26.6 tumours (Figure 6D).

By drawing ROIs over the whole tumour, TACs were obtained from the dynamic PET data sets (Figure 7). HT1080/26.6 tumours were characterised by a rapid delivery of [^{18}F]FETA up to 2 min p.i., followed by a plateau with a minimal increase of the TACs up to 60 min p.i. The delivery of the radiotracer into HT1080/1-3C tumours was comparatively slower, but retention was higher (Figure 7). The fractional retention of [^{18}F]FETA in tumours (ratio of radioactivity at 60 min to that at 2 min) was significantly higher in the 1-3C tumours compared to 26.6 tumours (1.44 ± 0.10 vs 1.10 ± 0.01; $P = 0.05$).

Biological basis and implication of [^{18}F]FETA retention in HT1080 tumours

In order to explain the differences in [^{18}F]FETA retention between the different HT1080 tumour types, we compared the retention of [^{18}F]FETA in the tumours to vessel density, oxygenation, and radiation sensitivity. The vessel density measured in histological sections of the HT1080 tumours was significantly lower for the 1-3C subclone, which contains less VEGF (Collingridge *et al*, 2002), compared to the 26.6 subclone (Figures 8A–C). The lower vessel density in the 1-3C tumours was associated with a significantly higher frequency of pO_2 values <1 mmHg (Figure 8D). Radiation sensitivity was determined for the two tumour types by measuring the fraction of clonogenic
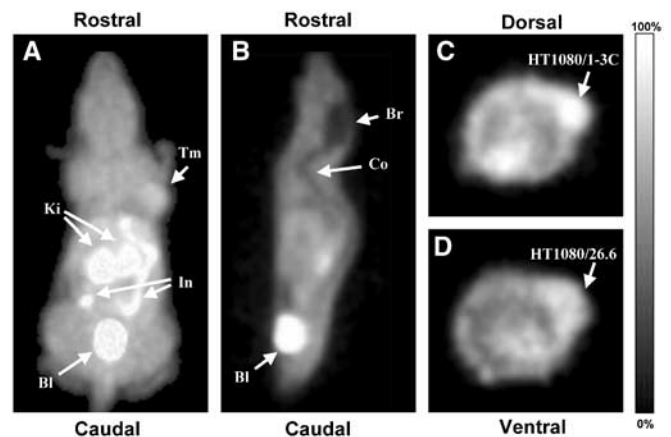
Figure 6 [^{18}F]FETA-PET images of HT1080 tumour-bearing mice acquired on the small animal quad-HIDAC scanner (pixel size 0.5 × 0.5 × 0.5 mm^3). (**A**) Three-dimensional (volume-rendered) image of an HT1080/1-3C tumour-bearing mouse (30–60 min p.i. summed) showing a dorsal view of the mouse. Here, pixel values are defined by the maximum voxel value in corresponding lines in the z-axis. Arrows point to tumour (Tm), Kidneys (Ki), small intestine (In), and urinary bladder (Bl). (**B**) Sagittal (0.5 mm) slice of 30–60 min p.i. summed [^{18}F]FETA-PET images from the same mouse as in (**A**) at the midplane level, showing low radiotracer uptake in brain (Br) and spinal cord (Co), as well as high accumulation in urinary bladder. (**C**) Transverse (0.5 mm) slice of 30–60 min p.i. summed [^{18}F]FETA-PET images from the same HT1080/1-3C tumour-bearing mouse as in (**A**) at the level of the maximal tumour diameter. (**D**) Corresponding transverse slice from an HT1080/26.6 tumour-bearing mouse, exhibiting lower tumour radiotracer uptake.
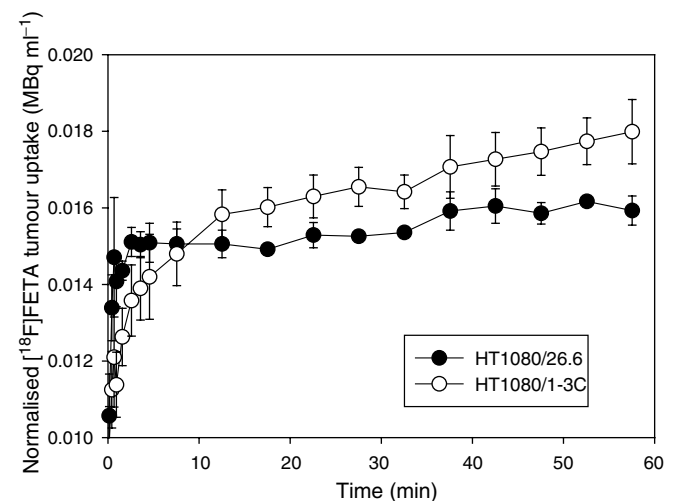

Figure 7 Tumour time–activity curves (TACs), normalised to the integral of the heart cavity TAC. The curves were obtained from region of interest analysis of dynamic [^{18}F]FETA-PET images from HT1080/26.6 (-●-) and HT1080/1-3C (-○-) tumour-bearing mice. Data are mean ± s.e.m. ($n = 3-4$ per group).

radiobiological hypoxic cells. The plating efficiency (mean ± s.e.m.) of HT1080/1-3C and /26.6 tumours were 0.50 ± 0.03 and 1.70 ± 0.41%, respectively. Overall, disaggregation of the tumours yielded (irradiated vs control) 2 to 20 × 10^6 cells vs 4 to 20 × 10^6 cells for HT1080/1-3C and 1 to 11 × 10^6 and 2 to 9 × 10^6 cells for HT1080/26.6 cells, respectively. Figures 8E, F show that hypoxic fraction was significantly higher in HT1080/1-3C than in HT1080/26.6 tumours (86.1 ± 2.1 vs 68.1 ± 0.2%, $P = 0.008$; Figures 8E, F).
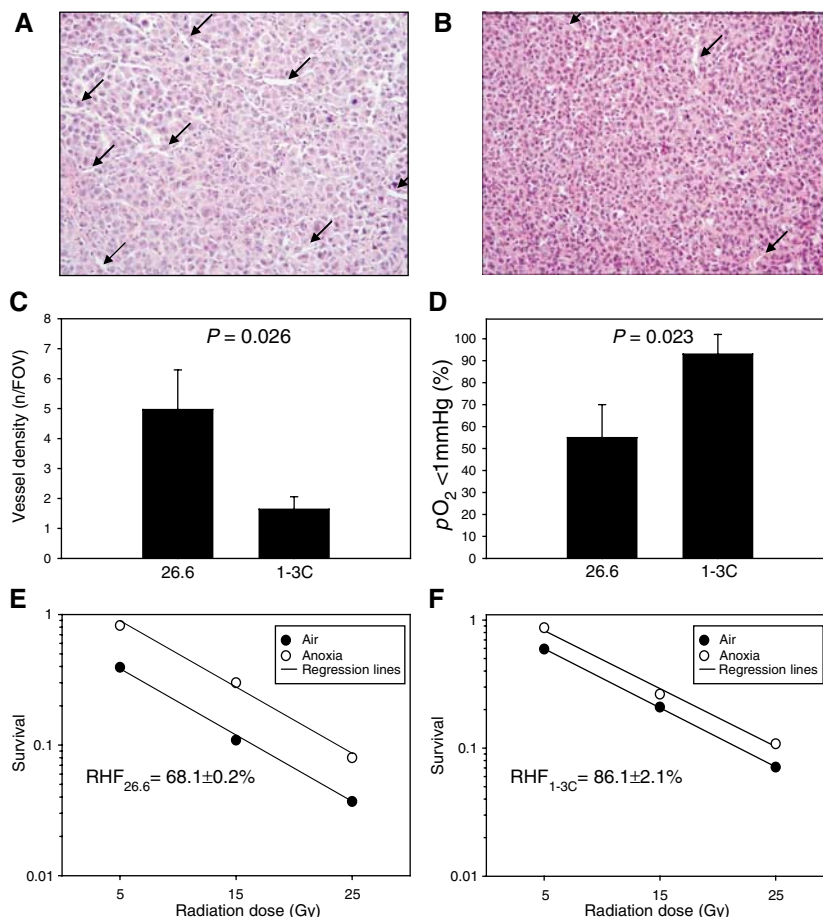
Figure 8 Vessel density, pO_2, and radiation sensitivity of HT1080/26.6 and HT1080/1-3 tumours. (**A–B**) Typical 5 μm H&E-stained histological sections of HT1080/26.6 (**A**) and HT1080/1-3C (**B**) tumours, with arrows pointing to vessels. (**C**) Summary data for vessel density depicting average number of vessels from five randomly selected fields of view (0.23 mm^2; × 200 magnification) per section; three sections per tumour. (**D**) OxyLite pO_2 measurements. (**E–F**) Radiation sensitivity determined in clonogenic assays and expressed as radiobiological hypoxic fraction of HT1080/26.6 (**E**) and HT1080/1.3C (**F**) tumours. Data are mean survival ($n = 4$). RHF, radiobiological hypoxic fraction. There was a statistically significant difference between the RHF of 1-3C and 26.6 tumours ($P = 0.008$).

DISCUSSION

The partial pressure of oxygen has been directly determined in accessible tumours such as cervix tumours, head and neck tumours, and sarcomas using Eppendorf oxygen electrodes (Höckel *et al*, 1996; Brizel *et al*, 1997; Nordsmark and Overgaard, 2000; Fyles *et al*, 2002). Such studies provided proof that low pO_2 (hypoxia) leads to poor outcome after cancer treatment. These findings, together with the well-known effect of hypoxia on radiation sensitivity as well as the development of hypoxia-modifying therapies, have strengthened the medical need for a noninvasive, clinically acceptable method of measuring hypoxia in patient tumours. Of the numerous possibilities available, the use of appropriately labelled 2-nitroimidazoles detectable by PET imaging is particularly attractive. In this paper, we have demonstrated that [^{18}F]FETA is a suitable radiotracer for PET imaging of tumour hypoxia.

^{18}F-labelled 1-(2-nitro-imidazolyl)-3-fluoro-2-propanol ([^{18}F]fluoromisonidazole ([^{18}F]FMISO) (Jerabek *et al*, 1986; Koh *et al*, 1995; Rasey *et al*, 1996)) is the most widely studied radiotracer for tumour hypoxia. This radiotracer has, however, failed to gain a wider acceptance for routine clinical application in a PET setting because of a number of limitations including: (i) slow accumulation in hypoxic tumours (scanning has been performed up to 5 h p.i. (Nunn *et al*, 1995; Bentzen *et al*, 2002)); (ii) low

target-to-background contrast due to high nonspecific binding resulting from a relatively high lipophilicity (octanol/water partition coefficient = 0.41 (Workman and Brown, 1981)); and (iii) significant non-oxygen-dependent metabolism (e.g. 50.0 and 36.2% of metabolites in plasma and urine, respectively, at 2 h p.i. (Rasey *et al*, 1999)). The choice of an ideal hypoxia marker would favour probes that have low lipophilicity and resistance to hypoxia-independent degradation; in general 2-nitroimidazoles with an amide side chain typified by etanidazole are more stable to nonhypoxic metabolism than those with a hydroxypropyl side chain such as misonidazole (Aboagye *et al*, 1998). [^{18}F]FETA possesses these favourable characteristics. Its octanol–water partition coefficient, determined here to be 0.16, is higher than nonfluorinated etanidazole (0.046 (Brown and Workman, 1980)), but lower than that of [^{18}F]FMISO. *In vitro*, [^{18}F]FETA accumulated selectively in hypoxic, but not in aerobic RIF-1 cells (4.3-fold differential at 120 min p.i.), consistent with the presence of a 2-nitroimidazole moiety (with redox potentials ($E_{1/7}$) around -380 to -390 mV (Adams *et al*, 1979; Brown and Workman, 1980; Workman and Brown, 1981). The large variation in uptake could be due to the differences in stable etanidazole levels in the reaction mixture.

[^{18}F]FETA accumulated in all tissues analysed. The retention of the radiotracer at 60-min postinjection was relatively low ($<$5% ID g^{-1}) in lung, heart, brain, and bone; intermediate (5–8%

Experimental Therapeutics

ID g^{-1}) in plasma, liver, spleen, small intestines, and muscle; and high (>8% ID g^{-1}) in kidney, bile, and urine. The highest [18F]FETA accumulation was found in the excretory organs. Good accumulation in tumours, 6–10% ID g^{-1}, would suggest the possibility of achieving high tumour-to-background contrast in several tumour types, including breast, lung, head and neck, and brain tumours. Chromatographic analysis of plasma, urine, and tissues provided some explanation for the differences in tissue distribution. [18F]FETA was found to be stable in plasma (~93% as parent compound at 60 min p.i.) and also excreted mainly as the unchanged drug in urine (74% at 60 min p.i.). The radiotracer was metabolised in liver to catabolite(s), which appeared to be eliminated predominantly via the hepatobiliary route.

Having shown that [18F]FETA is taken up into all tissues, we investigated whether differences in pO_2 could be monitored with the radiotracer *in vivo*. Two validation scenarios were explored. In the first instance, the 60-min retention of [18F]FETA into all tumour types as determined by γ-counting was compared to measured pO_2. Radiotracer retention positively correlated with the percentage of pO_2 values <5 mmHg ($r = 0.805$, $P = 0.027$), indicating that [18F]FETA retention is related to pO_2 levels. Using five different tumour types enabled a wide range of oxygenation levels to be achieved (the relative frequency of pO_2 values <1.0 mmHg ranged from 28 ± 13 to $93 \pm 9\%$ ($P = 0.008$; one-factorial ANOVA), and the relative frequency of pO_2 values <2.5 mmHg in a range from 51 ± 13 to $100 \pm 0\%$ ($P = 0.057$)). In general, the binding of nitroimidazoles requires the presence of nitroreductases, particularly cytochrome $P450$ reductase. We found no relationship between [18F]FETA and levels of the nitroreductases studied. Large differences in nitroreductase levels can confound measurement of hypoxia with 2-nitroimidazole-based probes; thus, our findings of a lack of significant differences in nitroreductase activities between the tumour types used is a relevant contribution to the interpretation of [18F]FETA data. The range of nitroreductase levels observed here, ≤2.5-fold, is unlikely to influence radiotracer retention due to a square-root relationship between the binding of 2-nitroimidazoles and cytochrome $P450$ reductase levels (Joseph *et al*, 1994). Rasey *et al* (1999) have shown that the half-maximal inhibition of [18F]FETA binding by oxygen is fairly similar (up to two-fold) across cell lines *in vitro*. This observation may be explained by the small differences in nitroreductase levels between cell lines. In the second instance, we investigated the ability of [18F]FETA to detect acute changes in tumour oxygenation. Carbogen breathing decreased the 60-min tumour retention of [18F]FETA by 36%, in keeping with an 11% decrease of hypoxic pO_2 values measured by OxyLite electrodes. This finding is similar to those reported previously for other 2-nitroimidazoles (Aboagye *et al*, 1997b, 1998; Rasey *et al*, 2000; Bentzen *et al*, 2002; Seddon *et al*, 2002) and demonstrates that [18F]FETA can be used to detect acute changes in pO_2.

PET studies performed in tumour-bearing mice demonstrated the feasibility of imaging hypoxia *in vivo*. Qualitatively, the PET images were in agreement with the quantitative tissue radioactivity data determined by γ-counting. It was also possible to perform semiquantitation of the dynamic PET data by ROI analysis. Interestingly, the tumour model with higher VEGF-expression (HT1080/26.6) showed lower fractional retention of the radiotracer compared to that with the lower VEGF-expression (HT1080/1-3C) despite a higher delivery of [18F]FETA into the former. This finding is in contradiction to the current dogma of 'hypoxia

inducing VEGF through the expression of HIF-1α' (Harris, 2002; Semenza, 2003) and, thus the more hypoxic tumours being those exhibiting higher levels of VEGF expression. This observation may be explained in part by the lower (~10-fold half-maximal inhibition) oxygen levels required to effect binding of 2-nitroimidazoles to cellular macromolecules *vs* that required to induce VEGF production (Leith and Michelson, 1995); in this regard, both tumour models are sufficiently hypoxic to induce VEGF production. The findings were, however, corroborated by a higher vessel density (explaining the higher radiotracer delivery) and a higher pO_2 (explaining the lower fractional retention) in the HT1080/26.6 model. The impact of these findings on radiation sensitivity was that the HT1080/26.6 tumours were more sensitive to radiation than the HT1080/1-3C tumours as demonstrated by a lower clonogenic radiobiological hypoxic fraction of the former. Since the pO_2 (and radiobiological hypoxic fractions) of the human tumour models used in this study have not been previously reported in the literature, an assessment of this (as well as the radiobiological hypoxic fraction for the HT1080 tumours) was made; the high and low pO_2 values obtained for EMT6 and RIF-1 tumours, respectively (Moulder and Rockwell, 1984), corroborate our measurements.

Since the PET studies required the use of anaesthesia for immobilisation, all other *in vivo* studies were performed under anaesthesia. It is conceivable that most anaesthesia will decrease clearance of radiotracers from the body and give rise to a systematic increase in hypoxia levels within tumours. This may explain the very high percentage of pO_2 values <2.5 mmHg seen in our experiments. These conditions have, however, been successfully used in other hypoxia experiments in mice to demonstrate nitroimidazole retention in tumours (Aboagye *et al*, 1997b). In translating this work into clinical studies one needs to bear in mind the fact that patients would be un-anaesthetised. The level of oxygenation may therefore be higher than that measured for the mouse tumours.

In summary we have validated an advanced-generation 2-nitroimidazole marker of tumour hypoxia in the mouse. Our findings indicate that [18F]FETA has suitable physicochemical properties and is stable to nonhypoxic degradation *in vivo*. We have also demonstrated that the tumour retention of the radiotracer is related to pO_2 status and radiobiological hypoxia. These properties, as well as the ability to image hypoxia (pO_2 values at 1–10 mmHg) dynamically with PET at early time points are attractive features that support the clinical development of [18F]FETA.

REFERENCES

Aboagye EO, Kelson AB, Tracy M, Workman P (1998) Preclinical development and current status of the fluorinated 2-nitroimidazole hypoxia prob N-(2-hydroxy-3,3,3-trifluoropropyl)-2-(2-nitro-1-imidazolyl) acetamide (SR

4554, CRC 94/17): a non-invasive diagnostic probe for the measurement of tumor hypoxia by magnetic resonance spectroscopy and imaging, and by positron emission tomography. *Anti-Cancer Drug Des* **13**: 703–730

Aboagye EO, Lewis AD, Tracy M, Workman P (1997a) Bioreductive metabolism of the novel fluorinated 2-nitroimidazole hypoxia probe N-(2-hydroxy-3,3,3-trifluoropropyl)-2-(2-nitroimidazolyl) acetamide (SR-4554). *Biochem Pharmacol* 54: 1217–1224

Aboagye EO, Maxwell RJ, Kelson AB, Tracy M, Lewis AD, Graham MA, Horsman MR, Griffiths JR, Workman P (1997b) Preclinical evaluation of the fluorinated 2-nitroimidazole N-(2-hydroxy-3,3,3-trifluoropropyl)-2-(2-nitro-1-imidazolyl) acetamide (SR-4554) as a probe for the measurement of tumor hypoxia. *Cancer Res* 57: 3314–3318

Adams GE, Clarke ED, Flockhart IR, Jacobs RS, Sehmi DS, Stratford IJ, Wardman P, Watts ME, Parrick J, Wallace RG, Smithen CE (1979) Structure–activity relationship in the development of hypoxic cell radiosensitizers. I. Sensitization efficiency. *Int J Radiol Biol* 35: 133–150

Aebersold DM, Burri P, Beer KT, Laissue J, Djonov V, Greiner RH, Semenza GL (2001) Expression of hypoxia-inducible factor-1alpha: a novel predictive and prognostic parameter in the radiotherapy of oropharyngeal cancer. *Cancer Res* 61: 2911–2916

Barthel H, Cleij MC, Collingridge DR, Hutchinson OC, Osman S, He Q, Luthra SK, Brady F, Price PM, Aboagye EO (2003) 3′-deoxy-3′-[^{18}F]fluorothymidine as a new marker for monitoring tumor response to anti-proliferative therapy *in vivo* with positron emission tomography. *Cancer Res* 63: 3791–3798

Bentzen L, Keiding S, Horsman MR, Grönroos T, Hansen SB, Overgaard J (2002) Assessment of hypoxia in experimental mice tumours by [^{18}F]Fluoromisonidazole PET and pO2 electrode measurements. *Acta Oncol* 41: 304–312

Brizel DM, Scully SP, Harrelson JM, Layfield LJ, Bean JM, Prosnitz LR, Dewhirst MW (1996) Tumor oxygenation predicts for the likelihood of distant metastases in human soft tissue sarcoma. *Cancer Res* 56: 941–943

Brizel DM, Sibley GS, Prosnitz LR, Scher RL, Dewhirst MW (1997) Tumor hypoxia adversely affects the prognosis of carcinoma of the head and neck. *Int J Radiat Oncol Biol Phys* 38: 285–289

Brown JM, Workman P (1980) Partition coefficient as a guide to the development of radiosensitizers which are less toxic than misonidazole. *Radiat Res* 82: 171–190

Collingridge DR, Carroll VA, Glaser M, Aboagye EO, Osman S, Hutchinson OC, Barthel H, Luthra SK, Brady F, Bicknell R, Price P, Harris AL (2002) The development of [[(124)I]iodinated-VG76e: a novel tracer for imaging vascular endothelial growth factor *in vivo* using positron emission tomography. *Cancer Res* 62: 5912–5919

Collingridge DR, Rockwell S (2000) Pentoxifylline improves the oxygenation and radiation response of BA1112 rat rhabdomyosarcomas and EMT6 mouse mammary carcinomas. *Int J Cancer* 90: 256–264

Collingridge DR, Young WK, Vojnovic B, Wardman P, Lynch EM, Hill SA, Chaplin DJ (1997) Measurement of tumor oxygenation: a comparison between polarographic needle electrodes and a time-resolved luminescence-based optical sensor. *Radiat Res* 147: 329–334

Dachs GU, Patterson AV, Firth JD, Ratcliffe PJ, Townsend KM, Stratford IJ, Harris AL (1997) Targeting gene expression to hypoxic tumor cells. *Nat Med* 3: 515–520

Dardzinski BJ, Sotak CH (1994) Rapid tissue oxygen tension mapping using 19F inversion-recovery echo-planar imaging of perfluoro-15-crown-5-ether. *Magn Reson Med* 32: 88–97

Dehdashti F, Mintun MA, Lewis JS, Bradley J, Govindan R, Laforest R, Welch MJ, Siegel BA (2003) *In vivo* assessment of tumor hypoxia in lung cancer with 60Cu-ATSM. *Eur J Nucl Med Mol Imaging* 30: 844–850

Evans SM, Jenkins WT, Joiner B, Lord EM, Koch CJ (1996) 2-Nitroimidazole (EF5) binding predicts radiation resistance in individual 9L s.c. tumors. *Cancer Res* 56: 405–411

Fitzsimmons SA, Workman P, Grever M, Paull K, Camalier R, Lewis AD (1996) Reductase enzyme expression across the National Cancer Institute Tumor cell line panel: correlation with sensitivity to mitomycin C and EO9. *J Natl Cancer Inst* 88: 259–269

Fujibayashi Y, Taniuchi H, Yonekura Y, Ohtani H, Konishi J, Yokoyama A (1997) Copper-62-ATSM: a new hypoxia imaging agent with high membrane permeability and low redox potential. *Nucl Med* 38: 1155–1160

Fyles A, Milosevic M, Hedley D, Pintilie M, Levin W, Manchul L, Hill RP (2002) Tumor hypoxia has independent predictor impact only in patients with node-negative cervix cancer. *J Clin Oncol* 20: 680–687

Gräber TG, Osmanian C, Jacks T, Housman DE, Koch CJ, Lowe SW, Giaccia AJ (1996) Hypoxia-mediated selection of cells with diminished apoptotic potential in solid tumours. *Nature* 379: 88–91

Harris AL (2002) Hypoxia – a key regulatory factor in tumour growth. *Nat Rev Cancer* 2: 38–47

Hasegawa T, Rhee JG, Levitt SH, Song CW (1987) Increase in tumor pO2 by perfluorochemicals and carbogen. *Int J Radiat Oncol Biol Phys* 13: 569–574

Helmer KG, Han S, Sotak CH (1998) On the correlation between the water diffusion coefficient and oxygen tension in RIF-1 tumors. *NMR Biomed* 11: 120–130

Höckel M, Knoop C, Schlenger K, Vorndran B, Baussmann E, Mitze M, Knapstein PG, Vaupel P (1993) Intratumoral pO2 predicts survival in advanced cancer of the uterine cervix. *Radiother Oncol* 26: 45–50

Höckel M, Schlenger K, Aral B, Mitze M, Schafer U, Vaupel P (1996) Association between tumor hypoxia and malignant progression in advanced cancer of the uterine cervix. *Cancer Res* 56: 4509–4515

Höckel M, Vaupel P (2001) Tumor hypoxia: definitions and current clinical, biological, and molecular aspects. *J Natl Cancer Inst* 93: 266–276

Hollander PM, Ernster L (1975) Studies on the reaction mechanism of DT diaphorase. Action of dead-end inhibitors and effects of phospholipids. *Arch Biochem Biophys* 169: 560–567

Honess DJ, Bleehen NM (1995) Perfusion changes in the RIF-1 tumour and normal tissues after carbogen and nicotinamide, individually and combined. *Br J Cancer* 71: 1175–1180

Honess DJ, Hill SA, Collingridge DR, Edwards B, Brauers G, Powell NA, Chaplin DJ (1998) Preclinical evaluation of the novel hypoxic marker 99mTc-HL91 (Prognox) in murine and xenograft systems *in vivo*. *Int J Radiat Oncol Biol Phys* 42: 731–735

Horsman MR, Overgaard J (1992) Overcoming tumour radiation resistance resulting from acute hypoxia. *Eur J Cancer* 28A: 2084–2085

Hoskin PJ, Saunders MI (1994) ARCON. *Clin Oncol (Roy Coll Radiol)* 6: 281–282

Ilangovan G, Li H, Zweier JL, Krishna MC, Mitchell JB, Kuppusamy P (2002) *In vivo* measurement of regional oxygenation and imaging of redox status in RIF-1 murine tumor: effect of carbogen-breathing. *Magn Reson Med* 48: 723–730

Jeavons AP, Chandler RA, Dettmat CA (1999) A 3D HIDAC-PET camera with sub-millimetre resolution for imaging small animals. *IEEE Trans Nucl Sci* 46: 468–473

Jerabek PA, Patrick TB, Kilbourn MR, Dischino DD, Welch MJ (1986) Synthesis and biodistribution of 18F-labeled fluoronitroimidazoles: potential *in vivo* markers of hypoxic tissue. *Int J Radiat Appl Instrum (A)* 37: 599–605

Joseph P, Jaiswal AK, Stobbe CC, Chapman JD (1994) The role of specific reductases in the intracellular activation and binding of 2-nitroimidazoles. *Int J Radiat Oncol Biol Phys* 29: 351–355

Kaanders JH, Wijffels KI, Marres HA, Ljungkvist AS, Pop LA, van den Hoogen FJ, de Wilde PC, Bussink J, Raleigh JA, van der Kogel AJ (2002) Pimonidazole binding and tumor vascularity predict for treatment outcome in head and neck cancer. *Cancer Res* 62: 7066–7074

Koh WJ, Bergman KS, Rasey JS, Peterson LM, Evans ML, Graham MM, Grierson JR, Lindsley KL, Lewellen TK, Krohn KA, Griffin WG (1995) Evaluation of oxygenation status during fractionated radiotherapy in human nonsmall cell lung cancers using [F-18]fluoromisonidazole positron emission tomography. *Int J Radiat Oncol Biol Phys* 33: 391–398

Koong AC, Denko NC, Hudson KM, Schindler C, Swiersz L, Koch C, Evans S, Ibrahim H, Le QT, Terris DJ, Giaccia AJ (2000) Candidate genes for the hypoxic tumor phenotype. *Cancer Res* 60: 883–887

Leith JT, Michelson S (1995) Secretion rates and levels of vascular endothelial growth factor in clone A or HCT-8 human colon tumour cells as a function of oxygen concentration. *Cell Prolif* 28: 415–430

Mannan RH, Somayaji VV, Lee J, Mercer JR, Chapman JD, Wiebe LI (1991) Radioiodinated 1-(5-iodo-5-deoxy-beta-D-arabinofuranosyl)-2-nitroimidazole (iodoazomycin arabinoside: IAZA): a novel marker of tissue hypoxia. *J Nucl Med* 32: 1764–1770

Moulder JE, Rockwell S (1984) Hypoxic fractions of solid tumors: experimental techniques, methods of analysis, and a survey of existing data. *Int J Radiat Oncol Biol Phys* 10: 695–712

Nordsmark M, Overgaard J (2000) A confirmatory prognostic study on oxygenation status and loco-regional control in advanced head and neck squamous cell carcinoma treated by radiation therapy. *Radiother Oncol* 57: 39–43

Nordsmark M, Overgaard M, Overgaard J (1996) Pretreatment oxygenation predicts radiation response in advanced squamous cell carcinoma of the head and neck. *Radiother Oncol* 41: 31–39

Nunn A, Linder K, Strauss HW (1995) Nitroimidazoles and imaging hypoxia. *Eur J Nucl Med* 22: 265–280

Experimental Therapeutics

Powell ME, Collingridge DR, Saunders MI, Hoskin PJ, Hill SA, Chaplin DJ (1999) Improvement in human tumour oxygenation with carbogen of varying carbon dioxide concentrations. *Radiother Oncol* **50:** 167–171

Rasey JS, Casciari JJ, Hofstrand PD, Muzi M, Graham MM, Chin LK (2000) Determining hypoxic fraction in a rat glioma by uptake of radiolabeled fluoromisonidazole. *Radiat Res* **153:** 84–92

Rasey JS, Hofstrand PD, Chin LK, Tewson TJ (1999) Characterization of [18F]Fluoroetanidazole, a new radiopharmaceutical for detecting tumor hypoxia. *J Nucl Med* **40:** 1072–1079

Rasey JS, Koh WJ, Evans ML, Peterson LM, Lewellen TK, Graham MM, Krohn KA (1996) Quantifying regional hypoxia in human tumors with positron emission tomography of [18F]fluoromisonidazole: a pretherapy study of 37 patients. *Int J Radiat Oncol Biol Phys* **36:** 417–428

Rasey JS, Nelson NJ, Chin L, Evans ML, Grunbaum Z (1990) Characteristics of the binding of labeled fluoromisonidazole in cells *in vitro. Radiat Res* **122:** 301–308

Rockwell S, Moulder JE (1990) Hypoxic fractions of human tumors xenografted into mice: a review. *Int J Radiat Oncol Biol Phys* **19:** 197–202

Ruth T, Wolf A (1979) Absolute cross sections for the production of 18F via the 18O(p,n)18F reaction. *Radiochim Acta* **26:** 21–25

Seddon BM, Honess DJ, Vojnovic B, Tozer G, Workman P (2001) Measurement of tumor oxygenation: *in vivo* comparison of a luminescence fibre-optic sensor and a polarographic electrode in the P22 tumors. *Radiat Res* **55:** 837–846

Seddon BM, Maxwell RJ, Honess DJ, Grimshaw R, Raynaud F, Tozer GM, Workman P (2002) Validation of the fluorinated 2-nitroimidazole SR-4554 as a non-invasive hypoxia marker detected by magnetic resonance spectroscopy. *Clin Cancer Res* **8:** 2323–2335

Semenza GL (2003) Angiogenesis in ischemic and neoplastic disorders. *Annu Rev Med* **54:** 17–28

Sharp SY, Kelland LR, Valenti MR, Brunton LA, Hobbs S, Workman P (2000) Establishment of an isogenic human colon tumor model for NQO1 gene expression: application to investigate the role of DT-diaphorase in bioreductive drug activation *in vitro* and *in vivo. Mol Pharmacol* **58:** 1146–1155

Song CW, Lee I, Hasegawa T, Rhee JG, Levitt SH (1987) Increase in *p*O2 and radiosensitivity of tumors by Fluosol-DA (20%) and carbogen. *Cancer Res* **47:** 442–446

Sorger D, Patt M, Kumar P, Wiebe LI, Barthel H, Seese A, Dannenberg C, Tannapfel A, Sabri O (2003) 18F]Fluoroazomycinarabinofuranoside ((18)FAZA) and [(18)F]Fluoromisonidazole ((18)FMISO): a comparative study of their selective uptake in hypoxic cells and PET imaging in experimental rat tumors. *Nucl Med Biol* **30:** 317–326

Stratford IJ, Workman P (1998) Bioreductive drugs into the next millennium. *Anticancer Drug Des* **13:** 519–528

Tewson TJ (1997) Synthesis of [18F]fluoroetanidazole: a potential new tracer for imaging hypoxia. *Nucl Med Biol* **24:** 755–760

Vaupel P, Kallinowski F, Okunieff P (1989) Blood flow, oxygen and nutrient supply, and metabolic microenvironment of human tumors: a review. *Cancer Res* **49:** 6449–6465

Walton MI, Smith PJ, Workman P (1991) The role of NAD(P)H: quinone reductase (EC 1.6.99.2, DT-diaphorase) in the reductive bioactivation of the novel indoloquinone antitumor agent EO9. *Cancer Commun* **3:** 199–206

Wilson HK (2003) A simplified synthesis of 2,3,5,6-tetrafluorophenyl 2-(2-nitroimidazol-1-yl) acetate. *J Labelled Compound Radiopharm* **46:** 511–513

Winski SL, Hargreaves RH, Butler J, Ross D (1998) A new screening system for NAD(P)H : quinone oxidoreductase (NQO1)-directed antitumor quinones: identification of a new aziridinylbenzoquinone, RH1, as a NQO1-directed antitumor agent. *Clin Cancer Res* **4:** 3083–3088

Workman P (1982) Lipophilicity and the pharmacokinetics of nitroimidazoles. In *Advanced Topics on Radiosensitizers of Hypoxic Cells*, Breccia A, Rimondi C, Adams GE (eds). pp 143–163. Pienum Press: Amsterdam

Workman P, Brown JM (1981) Structure–pharmacokinetic relationships for misonidazole analogues in mice. *Cancer Chemother Pharmacol* **6:** 39–49

Workman P, Twentyman P, Balkwill F, Balmain A, Chaplin D, Double J, Embleton J, Newell D, Raymond R, Stables J, Stephens T, Wallace J (1998) United kingdom coordinating committee on cancer research (UKCCCR) guidelines for the welfare of animals in experimental neoplasia (second edition). *Br J Cancer* **77:** 1–10

Wykoff CC, Beasley NJ, Watson PH, Turner KJ, Pastorek J, Sibtain A, Wilson GD, Turley H, Talks KL, Maxwell PH, Pugh CW, Ratcliffe PJ, Harris AL (2000) Hypoxia-inducible expression of tumor-associated carbonic anhydrases. *Cancer Res* **60:** 7075–7083

Yang DJ, Wallace S, Cherif A, Li C, Gretzer MB, Kim EE, Podoloff DA (1995) Development of F-18-labeled fluoroerythronitroimidazole as a PET agent for imaging tumor hypoxia. *Radiology* **194:** 795–800

Young WK, Vojnovic B, Wardman P (1996) Measurement of oxygen tension in tumours by time-resolved fluorescence. *Br J Cancer* **27**(Suppl): S256–S259

Ziemer LS, Evans SM, Kachur AV, Shuman AL, Cardi CA, Jenkins WT, Karp JS, Alavi A, Dolbier Jr WR, Koch CJ (2003) Noninvasive imaging of tumor hypoxia in rats using the 2-nitroimidazole 18F-EF5. *Eur J Nucl Med Mol Imaging* **30:** 259–266